Elemental Mercury Concentrations and Fluxes in the Tropical Atmosphere and Ocean

Elemental mercury concentrations and fluxes in the tropical atmosphere and ocean

Anne L. Soerensen[a,b]*, Robert P. Mason[c], Prentiss H Balcom[c], Daniel J. Jacob[b], Yanxu Zhang[b], Joachim Kuss[d], Elsie M. Sunderland[a,b]

[a]Harvard School of Public Health, Department of Environmental Health, Boston MA, 02215, USA

[b]Harvard University, School of Engineering and Applied Sciences, Cambridge MA, 02138, USA

[c]University of Connecticut, Department of Marine Sciences, 1080 Sennecossett Road, Groton, CT, 0634, USA

[d]Department of Marine Chemistry, Leibniz Institute for Baltic Sea Research, Rostock, Germany

* Corresponding Author

Abstract

Air-sea exchange of elemental mercury (Hg^0) is a critical component of the global biogeochemical Hg cycle. To better understand variability in atmospheric and oceanic Hg^0, we collected high-resolution measurements across large gradients in temperature, salinity, and productivity in the Pacific Ocean (20°N-15°S). Surface seawater Hg^0 was much more variable than atmospheric concentrations. Peak seawater Hg^0 (~130 fM) observed in the inter-tropical convergence zone (ITCZ) were ~3-fold greater than surrounding areas (~50 fM), and are comparable to latitudinal gradients in the Atlantic Ocean. Peak evasion in the northern ITCZ was four times higher than surrounding oceanographic regimes and located where high wind speed and elevated seawater Hg^0 coincided. A modeling analysis using the MITgcm and atmospheric inputs from the GEOS-Chem global Hg model suggests that higher Hg inputs from enhanced precipitation in the ITCZ combined with the shallow ocean mixed layer in this region can explain observations. Modeled seawater Hg^0 concentrations reproduce the observed seawater Hg^0 peaks in the ITCZ of the Atlantic and Pacific Oceans but underestimate its magnitude, likely due to insufficient deep convective scavenging of oxidized Hg from the upper troposphere. Our results demonstrate the importance of scavenging of reactive mercury in the upper atmosphere driving variability in seawater Hg^0 and net Hg inputs to biologically productive regions of the tropical ocean.

Introduction

Air-sea exchange of elemental mercury (Hg^0) plays a critical role in the global mercury (Hg) cycle by extending the lifetime of anthropogenic Hg actively cycling in the environment.[1, 2] Most human exposure to methylmercury, a neurotoxin, is from pelagic species such as tuna harvested from the open ocean.[3, 4] Reduction of inorganic divalent mercury (Hg^{II}) in seawater to form Hg^0 and subsequent evasion to the atmosphere directly reduces the reservoir available for conversion to methylmercury.[5] Limited observational data on atmospheric and aquatic Hg^0 have hampered our ability to model air-sea exchange on a global scale and predict responses to changes in ocean biogeochemistry.[6, 7] Here we report new high-resolution data from the Pacific Ocean on atmospheric and aquatic Hg^0 concentrations measured across four oceanographic regimes identified by differences in temperature, salinity and productivity. We use these data to better understand environmental drivers of aqueous Hg^0 formation and evasion and discuss improvements to modeling capability motivated by these results and a previous study in the Atlantic.

Regional variability in Hg^0 evasion mainly reflects differences in turbulent mixing of the surface ocean (wind, bubbles, temperature) and Hg^0 concentrations in seawater.[8, 9] Atmospheric Hg^0 concentrations in the marine boundary layer are less variable than surface seawater.[6] Atmospheric deposition is the main source of Hg to the open ocean and plays a large role in determining the pool of Hg^{II} available for reduction.[8, 10] The remaining ~40% of global Hg inputs to the surface mixed layer of the ocean is from subsurface ocean upwelling, seasonal entrainment, and Ekman pumping.[11, 12]

Data on variability in Hg^0 concentrations in open ocean regions across large gradients in salinity, temperature, productivity, precipitation, and winds are severely limited. Early studies in

64 the Equatorial Pacific suggested that highest Hg^0 concentrations and associated evasion occur in
65 the most productive upwelling regions of the ocean due to enhanced biological reduction, but
66 spatial coverage of measurements was limited.[5, 13] More recent work suggests that photochemical
67 oxidation and reduction of Hg species occurs much faster than biotic reduction reactions, and
68 elevated ocean productivity may instead decrease seawater Hg^0 concentrations through enhanced
69 sorption and scavenging of particle associated Hg^{II} that would otherwise be reduced and
70 evaded.[6, 14, 15] Along a latitudinal transect of the Atlantic Ocean, *Kuss et al.*[16] found a strong
71 tropical maximum in Hg^0 concentrations associated with the inter-tropical convergence zone
72 (ITCZ) and significantly lower values in the equatorial upwelling zone, subtropics and mid-
73 latitudes. The authors attributed this spatial variability to a combination of high precipitation,
74 rapid Hg^{II} photoreduction due to intense solar radiation, and low wind speeds. Recent modeling
75 efforts have not captured this gradient in Hg^0 concentrations between the ITCZ and adjacent
76 areas[11] and some suggest elevated concentrations in upwelling regions.[12]
77 Here we analyze new data on Hg^0 concentrations measured across four biochemical
78 provinces of the Pacific Ocean, in combination with previously published data from the Atlantic
79 Ocean, to better understand factors driving spatial variability in aqueous Hg^0 concentrations. We
80 report high-resolution simultaneous measurements of atmospheric and aquatic Hg^0
81 concentrations along a latitudinal transect from ~20°N to ~15°S in the Pacific Ocean. These
82 measurements capture a large gradient in salinity, temperature, meteorology, productivity, and
83 oceanographic circulation. We use these data in combination with previously collected
84 information from the Atlantic Ocean to better understand factors driving latitudinal patterns in
85 seawater Hg^0 concentrations, and discuss implications for improving global air-sea exchange
86 estimates.

Methods

Field measurements

We collected high-resolution measurements of atmospheric and aquatic gaseous Hg^0 along the METZYME cruise track in the Pacific Ocean between 1-24 October 2011 from 20°N to 15°S (Figure 1). We measured atmospheric Hg^0 at a 5-minute resolution using a Tekran 2537A mercury vapor analyzer. The instrument was calibrated daily using the internal calibration source and had a detection limit of <0.2 ng m^{-3}. For aqueous Hg^0, we collected seawater from the ship's intake at 7 m depth and used the automatic continuous equilibrium system with a 5-minute temporal resolution of measurements as described in detail in *Andersson et al*.[17] The Tekran 2537B used during water sampling was also calibrated daily using the internal calibration source and the detection limit was <2 fM for seawater Hg^0.

We aggregated all high-resolution measurements including underway measurements of wind speed, salinity, temperature, precipitation, and *in situ* fluorescence (a proxy for algal productivity) into one-hour averages for statistical analyses. Averaging over an hour is reasonable as the short-term variability in the measurements was small. Dissolved gaseous Hg in surface seawater is assumed to be mainly Hg^0 because studies have shown that it generally contains <5% dimethylmercury.[18-20]

Modeling

Air-sea fluxes for field measurements were calculated using the Nightingale et al. [21] parameterization for instantaneous wind speeds, the Henry's law coefficient for Hg^0,[22] a temperature-corrected Schmidt number for CO_2,[23] and the Wilke-Chang method for estimation of

110 a temperature and salinity-corrected Hg^0 diffusivity[24]. A variety of values have been proposed
111 for the diffusivity of Hg^0, as discussed by Kuss et al.[25] and to demonstrate the impact of variation
112 in this parameter, the air-sea exchange estimate using their diffusivity parameterization is
113 included in the Table S1.[26] We selected the Nightingale et al.[21] parameterization because it
114 provides a mid-range estimate of air-sea exchange.[27, 28]

115 We compare observations to modeling results from the MIT General Circulation Model
116 (MITgcm)[29] driven by inputs from the GEOS-Chem model (version v9-01-02) using 2006-2009
117 meteorological data as described in *Zhang et al.*[30] and use the model results to look at total Hg
118 inputs and losses in the surface ocean mixed layer. The MITgcm has a horizontal resolution of
119 1°×1° and 23 vertical levels[31] and includes an ecological simulation of carbon and plankton
120 dynamics (the Darwin model).[32] Physical advection and diffusion of tracers are driven by ocean
121 circulation data from ECCO-GODAE state estimates.[33] Differences attributable to variability in
122 meteorological years of the observations are expected to be small (for wet deposition average
123 interannual variability between 2006-2011 was <5% for the Pacific (160°N transect) and the
124 Atlantic (25°W transect)).

125 The MITgcm includes both lateral and vertical transport of Hg species due to ocean
126 circulation and settling of suspended particles, as described in Zhang et al.[29, 34] The model was
127 run with repeated circulation and external forcing from current day rivers and deposition for 10
128 years.[35] Rate coefficients for photochemical and biologically driven redox reactions between Hg^0
129 and Hg^{II}, sorption to suspended particles, and parameterization of air-sea exchange estimates are
130 from published and previously evaluated models of Hg fate in the ocean.[11, 34]

131

132 **Results and Discussion**

We grouped observations across the METZYME cruise track into four oceanographic regimes representing: (1) the North Pacific (14-20°N), (2) the ITCZ (5-14°N), (3) the Equatorial Pacific (5°N-1°S), and (4) the South Pacific (1-15°S) (Figure 1, Figure S1). These are specified based on differences in ocean circulation and atmospheric processes, which are reflected in measureable difference in seawater temperature, salinity, and fluorescence [36] (Figure 2 ; Table 1). The regimes are dynamic and the spatial distribution changes with season. In the North Pacific, seawater is cold with characteristically low productivity. Approaching the ITCZ, seawater temperature increases and salinity declines as the result of high precipitation rates. The ITCZ also experiences substantial wind driven Ekman pumping and stratified surface waters. The equatorial region is dominated by the low temperatures of the South Equatorial Current and high productivity due to upwelling nutrients, while the South Pacific has warmer high salinity water with intermediate productivity.[37, 38]

Latitudinal variability in Hg^0

Table 1 and Figure 2 show measured atmospheric and aquatic Hg^0 concentrations along the cruise track, associated evasion fluxes, and ancillary data. Atmospheric Hg^0 concentrations are significantly elevated in the North Pacific (14-20°N) and ITCZ (5-14°N) compared to the equatorial (1-5°N) and South Pacific (1-15°S) (Tukey-Kramer test, $p<0.001$). Mean concentrations ranged from 1.15 ng m^{-3} in the South Pacific up to 1.32 ng m^{-3} in the North Pacific (Table 1). This pattern is consistent with enrichment of atmospheric mercury in the northern hemisphere from anthropogenic sources, as discussed elsewhere.[39, 40]

Studies conducted prior to the availability of our present analytical capability for high resolution measurements of aquatic and atmospheric Hg^0 suggested enhanced Hg^0 in equatorial

upwelling regions.[13] By contrast, we observed relatively low concentrations of atmospheric Hg^0 (mean 1.18 ng m^{-3}) and aquatic Hg^0 (mean 53 fM) in the equatorial region (1-5°N) compared to more northern oceanographic regimes. High Chl*a* and fluorescence in the equatorial region (Table 1) supports the premise that enhanced removal of Hg^{II} associated with suspended particles is likely occurring, lowering the Hg^{II} pool available for reduction and associated Hg^0 concentrations.

Seawater Hg^0 concentrations differ by almost a factor of three compared to <20% for atmospheric Hg^0. Concentrations were highest in the warm, low salinity waters of the ITCZ (~130 fM) and remained low and fairly stable outside this region (~47-53 fM). This variability is much higher than during four cruises over two years in the vicinity of Bermuda where the average concentration varied by less than a factor of two across cruises.[6] We attribute high concentrations observed in the oceanographic regime characteristic of the ITCZ to a combination of high Hg inputs through wet deposition and a shallow mixed layer in this region, the latter making elevated inputs more pronounced (Table 1).

Previously reported total Hg concentrations in wet deposition from across the Pacific (14-75 pM[40-42]) are ~50 times higher than seawater concentrations. Seawater Hg^0 and salinity were strongly anti-correlated (R^2=0.63) across the cruise. Precipitation rates in the ITCZ (2.5-3.0 m yr^{-1}) are much higher than adjacent areas (0.3-1.0 m yr^{-1}) (Figure S2).[43] Deep convective precipitation scavenges upper tropospheric air enriched in Hg^{II}, resulting in high rainwater concentrations.[44] A study from the Western Pacific region with deep convection reports an average summertime concentration of total Hg in wet deposition of ~58 pM.[45]

Seawater Hg^0 also varied significantly within the ITCZ (t-test, p<0.001), increasing south of 8°N (shaded areas on Figure 2) due to a combination of higher inputs from precipitation and

significantly lower wind speeds (t-test, $p<0.001$). Satellite data show an average rainfall of 1-3 mm h^{-1} during the cruise in the southern part of the ITCZ and little precipitation in the northern part[46] (Figure S2). The presence of a vertical salinity gradient in the mixed layer in the southern ITCZ but not the northern part supports this premise (Figure S3) and indicates that the ITCZ is moving south. Precipitation of 2 mm h^{-1} with 50 pM Hg concentrations over just one day (48 mm d^{-1}) would increase seawater Hg concentration within the upper 10 meters by ~25%, assuming a background concentration of ~1 pM.[47] Sustained precipitation over several days in the southern part of the ITCZ could, therefore, easily explain the observed increase concentrations in the entire mixed layer (~30 m).

Atmospheric Hg^0 is elevated in the northern part of the ITCZ temporarily influenced by the North Eastern trade winds, likely due to the highest evasion fluxes of the cruise observed in this region (>8 ng m^{-2} h^{-1}). Lower seawater Hg^0 is also apparent in the northern ITCZ compared to southern regions but the observed gradient in concentrations is likely attributable to differences in inputs (wet deposition) rather than losses as discussed above. The rapid equilibrium established between Hg^{II} and Hg^0 in surface waters[14] means that changes in Hg^0 concentrations reflect variability in the larger pool of inorganic Hg species. The relative increase in evasion in the northern ITCZ is thus not large enough to explain the observed north-south ITCZ gradient in seawater Hg^0.

Latitudinal variability in evasion

Air-sea exchange in the northern part of the ITCZ (maximum: 8.73 ng m^{-2} h^{-1}) was more than four-fold greater (mean: 3.24±2.22 ng m^2 h^{-1}) than in the more southerly oceanographic regimes (0.7-0.8 ng m^{-2} h^{-1}) and more than two-fold greater than in the North Pacific (Table 1).

These differences are due to a combination of high seawater Hg^0 and the North Eastern trade winds temporarily overlapping with the northern part of the ITCZ during our cruise (Figure 2). Wind speeds throughout the cruise were lowest between 8-12°S (<3 m s^{-1}), fairly stable between 8°S-4°N, dipped below 3 m s^{-1} again in the southern part of the ITCZ and then rapidly increased to 12 m s^{-1} in the northern regions (Figure 2). Although highest overall Hg^0 concentrations occurred in the southern part of the ITCZ, highest evasion fluxes are located in the northern region where high wind speeds (associated with southwards movement of the ITCZ) and elevated seawater Hg^0 coincide. Low seawater Hg^0 concentrations in the North Pacific between 12-15°N resulted in lower evasion despite high wind speeds. These observations reinforce the importance of understanding variability in seawater Hg^0 as a control on the magnitude of air-sea exchange, a factor that has been neglected in some broad scale studies.[48]

Large scale drivers of Hg^0 across ocean basins

Similar latitudinal variability in seawater Hg^0 is apparent by comparing data from the Pacific Ocean reported here to data from the Atlantic Ocean[16] (Figure 3). Kuss et al.[16] also observed elevated Hg^0 concentrations in the low salinity, warm waters of the Equatorial Atlantic Ocean across two seasons. Peak seawater Hg^0 in the Atlantic Ocean tracked the movement of the ITCZ between sampling periods in November and May (Figure 3). High Hg^0 concentrations in the ITCZ in the Atlantic springtime (~130 fM) were similar to those reported here for the Pacific (~130 fM), while concentrations measured during the Atlantic fall were higher (~220 fM). Hg^0 concentrations in the tropical Atlantic (15S-15N) ranged between 35-60 fM and also matched observations reported for the Pacific here (~50 fM). Variability in evasion fluxes was similar for

224 the Atlantic and Pacific ranging ~4 fold across regions with highest fluxes where high wind
225 speeds and elevated Hg^0 coincide in the tropical and subtropical oceans.

226 Figure 3 compares simulated Hg^0 using the MITgcm in surface seawater (0-10 m depth)
227 to observations from all three cruise transects. The model reproduces much of the observed
228 latitudinal variability in aqueous Hg^0 but only captures 45-70% of the amplitude of the peak in
229 the ITCZ. Kuss et al.[16] suggested that a combination of a shallow mixed layer and high solar
230 radiation could cause the elevated Hg^0 concentrations in the ITCZ but these processes are
231 accounted for in our model simulation.[11, 29]

232 Concentrations of Hg^0 in the surface ocean reflect the overall pool of inorganic Hg
233 because there is a rapid equilibrium established between Hg^0 and Hg^{II} in seawater, as discussed
234 above.[14] Figure 4 shows the relative importance of various input and loss pathways for inorganic
235 Hg in the surface ocean of the cruise regions sampled. Net inputs from atmospheric deposition
236 are the predominant source in the ITCZ across the Atlantic and Pacific regions. A sensitivity
237 simulation shows that modeled seawater Hg^0 is almost proportionally affected by changes in
238 atmospheric Hg^{II} inputs in the ITCZ (20% change in deposition resulted in 14-16% change in
239 Hg^0 in the ITCZ and 6-16% elsewhere; Figure S4). Thus, low bias in modeled seawater Hg^0 in
240 the ITCZ compared to observations likely reflects insufficient Hg deposition in the atmospheric
241 simulation (GEOS-Chem) for this region.

242 The GEOS-Chem model reproduces the precipitation rate in the ITCZ fairly well
243 compared to satellite observations[46] suggesting the model underestimation is related to limited
244 supply of Hg^{II} in the atmosphere. Deep convective cloud systems and high precipitation loads
245 distinguish the ITCZ from other parts of the tropical ocean[43, 49] and recent work has shown that
246 cumulonimbus clouds reaching altitudes of 10-14 km may enhance Hg^{II} scavenging compared to

stratiform clouds (~4 km) for the same precipitation load.[50] Insufficient deposition in areas of deep convection has also been noted in comparisons of GEOS-Chem simulated deposition to measured Hg wet deposition from the MDN network data at mid latitudes.[30, 51] In both the mid-latitudes and the tropics this discrepancy could be caused by model underestimation of upper tropospheric Hg^{II}, which is supported by recent observations,[52] or insufficient model scavenging of the upper troposphere. As evidence for the latter, Wang et al.[53] found that GEOS-Chem greatly overestimates upper tropospheric black carbon concentrations in the tropics. Our work suggests the need for additional measurements of wet deposition in tropical areas and improved understanding of atmospheric Hg dynamics in regions with deep convection to better quantify mercury deposition and resulting seawater concentrations in the tropics.[54]

Figure 4 illustrates the importance of lateral seawater flow in the surface ocean for redistributing enhanced atmospheric mercury deposited in the ITCZ region. Ekman pumping is particularly pronounced in the oceanographic regime that reflects the influence of the ITCZ, resulting in strong horizontal outflow of Hg in the surface ocean to other regions of the tropical ocean. Upwelling in the equatorial region and along the African coast reintroduces Hg from the subsurface ocean into the surface ocean.[55, 56] In highly productive regions such as the Patagonian Shelf in the Atlantic, losses from particle settling can exceed evasion. These results clearly illustrate the importance of adequately capturing both Hg redox chemistry and physical transport processes in the atmosphere and ocean to resolve air-sea exchange estimates. Results presented here suggest enhanced atmospheric Hg inputs in the ITCZ are redistributed through lateral ocean transport of surface waters (Figure 4) to biologically productive regions of the tropical ocean.

Supporting Information

Additional information, including all data for atmospheric and aquatic Hg^0 from the Atlantic and Pacific Oceans and associated evasion fluxes are available free of charge via the Internet at http://pubs.acs.org.

Acknowledgements

We acknowledge financial support from the U.S. National Science Foundation, Chemical Oceanography division (NSF OCE-1130549). ALS acknowledges financial support from the Carlsberg Foundation. We thank the captain, science technicians, and crew of the *RV Kilo Moana*. And Carl Lamborg and Mak Saito (WHOI) for allowing us to participate in their cruise onboard the *RV Kilo Moanai*. We thank Elizabeth S. Corbitt, Helen Amos, and Johan Schmidt for helpful discussions.

References

1. Corbitt, E. S.; Jacob, D. J.; Holmes, C. D.; Streets, D. G.; Sunderland, E. M. Global Source-Receptor Relationships for Mercury Deposition under Present-Day and 2050 Emissions Scenarios. *Environ. Sci. Technol.* **2011,** *45*, (24), 10477-10484; DOI 10.1021/Es202496y.
2. Amos, H. M.; Jacob, D. J.; Streets, D. G.; Sunderland, E. M. Legacy Impacts of All-Time Anthropogenic Emissions on the Global Mercury Cycle. *Biogeochem. Cycles* **2013,** *27*, 1-12; DOI 10.1002/gbc.20040.
3. Sunderland, E. M. Mercury Exposure from Domestic and Imported Estuarine and Marine Fish in the Us Seafood Market. *Environmental Health Perspectives* **2007,** *115*, (2), 235-242; DOI 10.1289/Ehp.9377.
4. Mahaffey, K. R.; Sunderland, E. M.; Chan, H. M.; Choi, A. L.; Grandjean, P.; Marien, K.; Oken, E.; Sakamoto, M.; Schoeny, R.; Weihe, P.; Yan, C. H.; Yasutake, A. Balancing the Benefits of N-3 Polyunsaturated Fatty Acids and the Risks of Methylmercury Exposure from Fish Consumption. *Nutr. Rev.* **2011,** *69*, (9), 493-508; DOI 10.1111/j.1753-4887.2011.00415.x.
5. Mason, R. P.; Fitzgerald, W. F. The Distribution and Biogeochemical Cycling of Mercury in the Equatorial Pacific-Ocean. *Deep-Sea Res., Part I* **1993,** *40*, (9), 1897-1924.
6. Soerensen, A. L.; Mason, R. P.; Balcom, P. H.; Sunderland, E. M. Drivers of Surface Ocean Mercury Concentrations and Air-Sea Exchange in the West Atlantic Ocean.

Environmental Science and Technology **2013,** *47*, 7757-7765; DOI 10.1021/ea401354q.
7. Doney, S. C. The Growing Human Footprint on Coastal and Open-Ocean Biogeochemistry. *Science* **2010,** *328*, (5985), 1512-1516.
8. Mason, R. P.; Sheu, G. R. Role of the Ocean in the Global Mercury Cycle. *Glob. Biogeochem. Cycles* **2002,** *16*, (4).
9. Andersson, M. E.; Sommar, J.; Gardfeldt, K.; Lindqvist, O. Enhanced Concentrations of Dissolved Gaseous Mercury in the Surface Waters of the Arctic Ocean. *Mar. Chem.* **2008,** *110*, (3-4), 190-194.
10. Sunderland, E. M.; Mason, R. P. Human Impacts on Open Ocean Mercury Concentrations. *Glob. Biogeochem. Cycles* **2007,** *21*, (4); Artn Gb4022; DOI 10.1029/2006gb002876.
11. Soerensen, A. L.; Sunderland, E. M.; Holmes, C. D.; Jacob, D. J.; Yantosca, R. M.; Skov, H.; Christensen, J. H.; Strode, S. A.; Mason, R. P. An Improved Global Model for Air-Sea Exchange of Mercury: High Concentrations over the North Atlantic. *Environ. Sci. Technol.* **2010,** *44*, (22), 8574-8580; DOI 10.1021/Es102032g.
12. Strode, S. A.; Jaegle, L.; Selin, N. E.; Jacob, D. J.; Park, R. J.; Yantosca, R. M.; Mason, R. P.; Slemr, F. Air-Sea Exchange in the Global Mercury Cycle. *Glob. Biogeochem. Cycles* **2007,** *21*, (1); DOI 10.1029/2006GB002766.
13. Fitzgerald, W. F.; Gill, G. A.; Kim, J. P. An Equatorial Pacific-Ocean Source of Atmospheric Mercury. *Science* **1984,** *224*, (4649), 597-599.
14. Qureshi, A.; O'Driscoll, N. J.; MacLeod, M.; Neuhold, Y. M.; Hungerbuhler, K. Photoreactions of Mercury in Surface Ocean Water: Gross Reaction Kinetics and Possible Pathways. *Environ. Sci. Technol.* **2010,** *44*, (2), 644-649; DOI 10.1021/es9012728.
15. O'Driscoll, N. J.; Siciliano, S. D.; Lean, D. R. S.; Amyot, M. Gross Photoreduction Kinetics of Mercury in Temperate Freshwater Lakes and Rivers: Application to a General Model of Dgm Dynamics. *Environ. Sci. Technol.* **2006,** *40*, (3), 837-843.
16. Kuss, J.; Zülicke, C.; Pohl, C.; Schneider, B. Atlantic Mercury Emission Determined from Continuous Analysis of the Elemental Mercury Sea-Air Concentration Difference within Transects between 50 Degrees N and 50 Degrees S. *Glob. Biogeochem. Cycles* **2011,** *25*.
17. Andersson, M. E.; Gardfeldt, K.; Wangberg, I. A Description of an Automatic Continuous Equilibrium System for the Measurement of Dissolved Gaseous Mercury. *Anal. Bioanal. Chem.* **2008,** *391*, (6), 2277-2282; DOI 10.1007/s00216-008-2127-4.
18. Whalin, L.; Kim, E.; Mason, R. Factors Influencing the Oxidation, Reduction, Methylation and Demethylation of Mercury Species in Coastal Waters. *Marine Chemistry* **2007,** *107*, 278-294.
19. Mason, R.; Rolfhus, K.; Fitzgerald, W. Methylated and Elemental Mercury Cycling in Surface and Deep-Ocean Waters of the North Atlantic. *Water Air and Soil Pollution* **1995,** *80*, (1-4), 665-677.
20. Mason, R. P.; Sullivan, K. A. The Distribution and Speciation of Mercury in the South and Equatorial Atlantic. *Deep-Sea Res., Part Ii* **1999,** *46*, (5), 937-956.
21. Nightingale, P. D.; Malin, G.; Law, C. S.; Watson, A. J.; Liss, P. S.; Liddicoat, M. I.; Boutin, J.; Upstill-Goddard, R. C. In Situ Evaluation of Air-Sea Gas Exchange

Parameterizations Using Novel Conservative and Volatile Tracers. *Glob. Biogeochem. Cycles* **2000,** *14*, (1), 373-387.
22. Andersson, M. E.; Gardfeldt, K.; Wangberg, I.; Stromberg, D. Determination of Henry's Law Constant for Elemental Mercury. *Chemosphere* **2008,** *73*, (4), 587-592; DOI 10.1016/j.chemosphere.2008.05.067.
23. Poissant, L.; Amyot, M.; Pilote, M.; Lean, D. Mercury Water-Air Exchange over the Upper St. Lawrence River and Lake Ontario. *Environ. Sci. Technol.* **2000,** *34*, (15), 3069-3078.
24. Wilke, C. R.; Chang, P. Correlation of Diffusion Coefficients in Dilute Solutions. *AIChE J.* **1955,** *1*, (2), 264-270.
25. Kuss, J.; Holzmann, J.; Ludwig, R. An Elemental Mercury Diffusion Coefficient for Natural Waters Determined by Molecular Dynamics Simulation. *Environ. Sci. Technol.* **2009,** *43*, (9), 3183-3186.
26. Kuss, J. Water–Air Gas Exchange of Elemental Mercury: An Experimentally Determined Mercury Diffusion Coefficient for Hg0 Water-Air Flux Calculations. *Limnology and Oceanography* **2014,** *59(5)*, 7.
27. Wanninkhof, R. Relationship between Wind-Speed and Gas-Exchange over the Ocean. *J. Geosphys. Res. Oceans* **1992,** *97*, (C5), 7373-7382.
28. Liss, P. S.; Merlivat, L. Air-Sea Exchange Rates: Introduction and Synthesis. In *The Role of Air-Sea Exchange in Geochemical Cycling*; Buat-Menard, P., Ed. Reidel Publishing Compant: Dodrecht, 1986; pp 113-127.
29. Zhang, Y.; Jacob, D. J.; Amos, H. M.; Dutkiewicz, S.; Sunderland, C. J. Transport and Fate of Riverine Discharged Mercury in the Ocean: Burial in Coasts and Contributions to Open Ocean Concentrations. *In prep* **2014**.
30. Zhang, Y.; Jaegle, L.; van Donkelaar, A.; Martin, R. V.; Holmes, C. D.; Amos, H. M.; Wang, Q.; Talbot, R.; Artz, R.; Brooks, S.; Luke, W.; Holsen, T. M.; Felton, D.; Miller, E. K.; Perry, K. D.; Schmeltz, D.; Steffen, A.; Tordon, R.; Weiss-Penzias, P.; Zsolway, R. Nested-Grid Simulation of Mercury over North America. *Atmos. Chem. Phys.* **2012,** *12*, (14), 6095-6111.
31. Marshall, J.; Hill, C.; Perelman, L.; Adcroft, A. Hydrostatic, Quasi-Hydrostatic, and Nonhydrostatic Ocean Modeling. *J. Geosphys. Res. Oceans* **1997,** *102*, (C3), 5733-5752.
32. Dutkiewicz, S.; Follows, M. J.; Bragg, J. G. Modeling the Coupling of Ocean Ecology and Biogeochemistry. *Glob. Biogeochem. Cycles* **2009,** *23*.
33. Wunsch, C.; Heimbach, P. Practical Global Oceanic State Estimation. *Physica D-Nonlinear Phenomena* **2007,** *230*, (1-2), 197-208.
34. Zhang, Y.; Jaegle, L.; Thompson, L. Natural Biogeochemical Cycle of Mercury in a Global Three-Dimensional Ocean Tracer Model. *Glob. Biogeochem. Cycles* **2014,** *Published online*; DOI: 10.1002/2014GB004814.
35. Amos, H. M.; Jacob, D. J.; Kochman, D.; Horowitz, H. M.; Zhang, Y.; Dutkiewicz, S.; Horvat, M.; Corbitt, E. S.; Sunderland, E. M., Global Biogeochemical Implications of Mercury Discharges from Tivers and Sediment Burial. In *Environmental Science and Technology*, Submitted.
36. Reygondeau, G.; Lonhurst, A.; Martinez, E.; Beaugrand, G.; Antoine, D.; Maury, O. Dynamic Biogeochemical Provinces in the Global Ocean. *Glob. Biogeochem. Cycles* **2013,** *27*, (1-13), 1-13; DOI 10.1002/gbc.20089.

37. Pennington, J. T.; Mahoney, K. L.; Kuwahara, V. S.; Kolber, D. D.; Calienes, R.; Chavez, F. P. Primary Production in the Eastern Tropical Pacific: A Review. *Progress in Oceanography* **2006,** *69*, (2-4), 285-317.
38. Pickard, G. L.; Emery, W. J., *Descriptive Physical Oceanography*. 5th edition ed.; Pergamon Press: 1990.
39. Slemr, F. Trends in Atmospheric Mercury Concentrations over the Atlantic Ocean and at the Wank Summit, and the Resulting Constraints on the Budget of Atmospheric Mercury. In *Global and Regional Mercury Cycles: Sources, Fluxes and Mass Balances*; Baeyens, W., Ed. Kluwer Academic Publishers: Netherlands, 1996; Vol. 21, pp 33-84.
40. Fitzgerald, W. F. Cycling of Mercury between the Atmosphere and Oceans. In *The Role of Air-Sea Exchange in Geochemical Cycling*; Buat-Menard, P., Ed. D. Reidel Publishing Company: 1986; Vol. 185, pp 363-408.
41. Mason, R. P.; Fitzgerald, W. F.; Vandal, G. M. The Sources and Composition of Mercury in Pacific-Ocean Rain. *Journal of Atmospheric Chemistry* **1992,** *14*, (1-4), 489-500.
42. Laurier, F. J. G.; Mason, R. P.; Whalin, L.; Kato, S. Reactive Gaseous Mercury Formation in the North Pacific Ocean's Marine Boundary Layer: A Potential Role of Halogen Chemistry. *Journal of Geophysical Research-Atmospheres* **2003,** *108*, (D17).
43. *NASA: Tropical Rainfall Measuring Mission (Trmm)* Website: http://pmm.nasa.gov/TRMM/TRMM-based-climatology (Access date: June 2014).
44. Selin, N. E.; Jacob, D. J. Seasonal and Spatial Patterns of Mercury Wet Deposition in the United States: Constraints on the Contribution from North American Anthropogenic Sources. *Atmospheric Environment* **2008,** *42*, (21), 5193-5204.
45. Sheu, G. R.; Lin, N. H. Characterizations of Wet Mercury Deposition to a Remote Islet (Pengjiayu) in the Subtropical Northwest Pacific Ocean. *Atmospheric Environment* **2013,** *77*, 474-481.
46. *RSS (Remote Sensing System): Remss* http://www.remss.com/missions/windsat (Access date: November 2013).
47. Sunderland, E. M.; Krabbenhoft, D. P.; Moreau, J. W.; Strode, S. A.; Landing, W. M. Mercury Sources, Distribution, and Bioavailability in the North Pacific Ocean: Insights from Data and Models. *Glob. Biogeochem. Cycles* **2009,** *23*; Artn Gb2010; DOI 10.1029/2008gb003425.
48. De Simone, F.; Gencarelli, C. N.; Hedgecock, I. M.; Pirrone, N. Global Atmospheric Cycle of Mercury: A Model Study on the Impact of Oxidation Mechanisms. *Environmental Science and Pollution Research* **2014,** *21*, 4110-4123; 10.1007/s11356-013-2451-x.
49. Hong, G.; Heygster, G.; Miao, J. G.; Kunzi, K. Detection of Tropical Deep Convective Clouds from Amsu-B Water Vapor Channels Measurements. *Journal of Geophysical Research-Atmospheres* **2005,** *110*, (D5).
50. Nair, U. S.; Wu, Y.; Holmes, C. D.; Ter Schure, A.; Kallos, G.; Walters, J. T. Cloud-Resolving Simulations of Mercury Scavenging and Deposition in Thunderstorms. *Atmos. Chem. Phys.* **2013,** *13*, (19), 10143-10157.
51. Holmes, C. D.; Jacob, D. J.; Corbitt, E. S.; Mao, J.; Yang, X.; Talbot, R.; Slemr, F. Global Atmospheric Model for Mercury Including Oxidation by Bromine Atoms. *Atmos. Chem. Phys.* **2010,** *10*, (24), 12037-12057.

52. Lyman, S. N.; Jaffe, D. A. Formation and Fate of Oxidized Mercury in the Upper Troposphere and Lower Stratosphere. *Nature Geoscience* **2012,** *5*, (2), 114-117.
53. Wang, Q. Q.; Jacob, D. J.; Spackman, J. R.; Perring, A. E.; Schwarz, J. P.; Moteki, N.; Marais, E. A.; Ge, C.; Wang, J.; Barrett, S. R. H. Global Budget and Radiative Forcing of Black Carbon Aerosol: Constraints from Pole-to-Pole (Hippo) Observations across the Pacific. *Journal of Geophysical Research-Atmospheres* **2014,** *119*, (1), 195-206.
54. Yuan, J. A.; Houze, R. A. Global Variability of Mesoscale Convective System Anvil Structure from a-Train Satellite Data. *Journal of Climate* **2010,** *23*, (21), 5864-5888.
55. Doi, T.; Tozuka, T.; Yamagata, T. Interannual Variability of the Guinea Dome and Its Possible Link with the Atlantic Meridional Mode. *Climate Dynamics* **2009,** *33*, (7-8), 985-998.
56. Huete-Ortega, M.; Calvo-Diaz, A.; Grana, R.; Mourino-Carballido, B.; Maranon, E. Effect of Environmental Forcing on the Biomass, Production and Growth Rate of Size-Fractionated Phytoplankton in the Central Atlantic Ocean. *J. Mar. Sys.* **2011,** *88*, (2), 203-213.

457 Table 1. Summary of observations across oceanographic regimes of the Pacific Ocean.

	North Pacific 14-20°N	ITCZ 5-14°N	Equator 1°S-5°N	South Pacific 1-15°S
Hg^0_{atm} (ng m^{-3})	1.32±0.1★	1.27±0.1★	1.18±0.1	1.15±0.1
Hg^0_{aq} (fM)	51.3±4.1★°	104.7±19.9	53.0±10.3★	47.0±13.3°
Hg^0 flux (ng m^2 h^{-1})	1.4±0.2	3.2±2.2	0.7±0.4★	0.8±0.4★
Wind Speed (m s^{-1})	9.8±2.5	6.6±2.9	5.1±1.2★	5.6±1.7★
Sea surface temperature (°C)	26.1±0.35	28.2±0.39★	26.9±0.70	28.3±0.51★
Salinity (psu)	35.0±0.02	34.3±0.15	35.1±0.11	35.7±0.17
Fluorescence (unitless)[A]	99.7±2.6	116.3±23.6	209.3±50.7	139.3±42.3
Chl*a* (mg m^{-3})	0.03-0.06	0.06-0.09	0.12-0.27	0.06-0.15
Mixed layer depth (m)	50	30	100	150

458 All regions are significantly different from each other using a Tukey-Kramer test for multiple comparisons unless
459 denoted ★ or °.
460 [A] Fluorescence was measured with a baseline ~95 and provides a relative indicator of variability in productivity
461 across the cruise track but cannot be compared between cruises because the baseline value is cruise specific.
462
463

Figure captions

Figure 1. Oceanographic regimes sampled on the METZYME cruise and measured seawater Hg^0 concentrations.

Figure 2. Latitudinal variability in measured atmospheric and seawater Hg^0 concentrations, associated evasion, and environmental properties on the METZYME cruise between 1-24 October, 2011. Oceanographic regimes for October 2011 are shown; shaded areas denote statistically different regions for Hg^0 concentrations within the oceanic regime reflecting the ITCZ.

Figure 3. Comparison of modeled (red) and observed (blue) latitudinal gradients in Hg^0 along cruise tracks in the Pacific and the Atlantic Oceans. Model results are from the MITgcm within ±2 degrees of the cruise track with atmospheric inputs from the GEOS-Chem global Hg model. Data from the Atlantic Ocean are from Kuss et al.[16]

Figure 4. Modeled inputs and losses of Hg in the ocean mixed layer across the cruise regions sampled. Results are presented as monthly averages from the MITgcm Hg simulation.[29] Model comparison with observations indicates a low bias in atmospheric inputs in the ITCZ (Figure 3). Specifications of the budget calculations reported here are provided in the SI.

TOC-ART

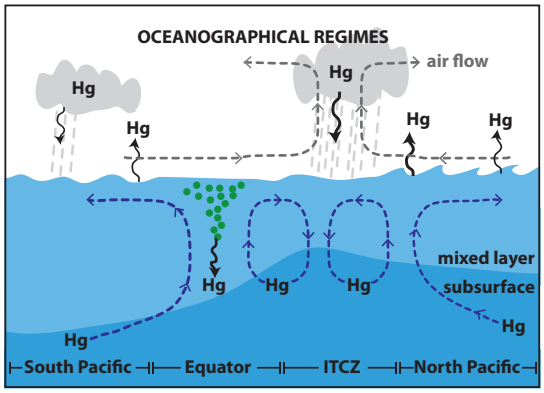
OCEANOGRAPHICAL REGIMES
air flow
Hg
Hg
Hg
Hg
Hg
Hg
Hg
Hg
Hg
Hg
mixed layer
subsurface
South Pacific
Equator
ITCZ
North Pacific

486

487
488

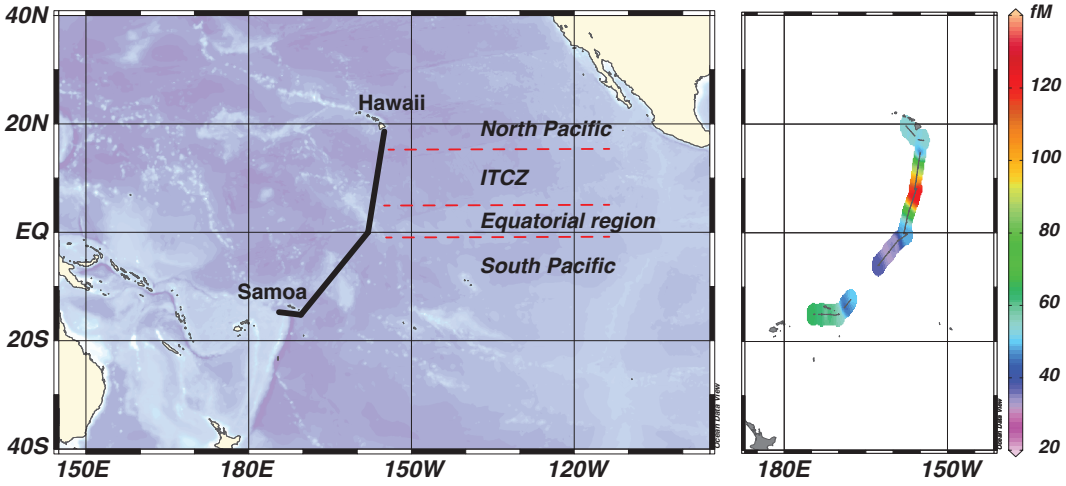

Figure 1. Oceanographic regimes sampled on the METZYME cruise and measured seawater Hg0 concentrations.

489
490

491
492

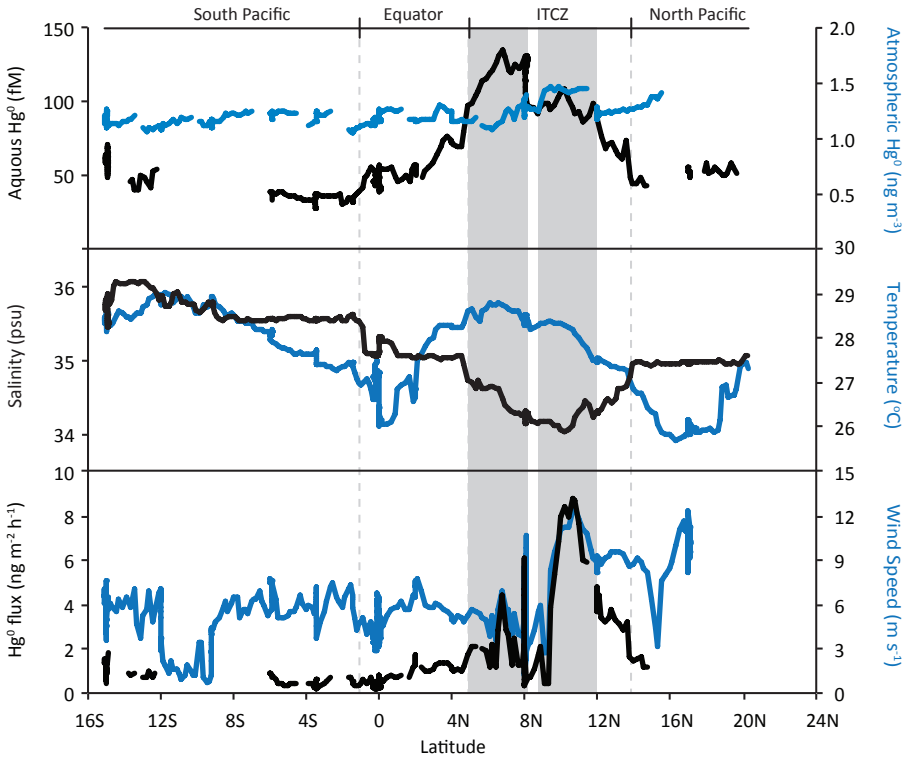

Figure 1. Latitudinal variability in measured atmospheric and seawater Hg0 concentrations, associated evasion, and environmental properties on the METZYME cruise between 1-24 October, 2011. Oceanographic regimes for October 2011 are shown; shaded areas denote statistically different regions for Hg0 concentrations within the oceanic regime reflecting the ITCZ.

493
494
495
496

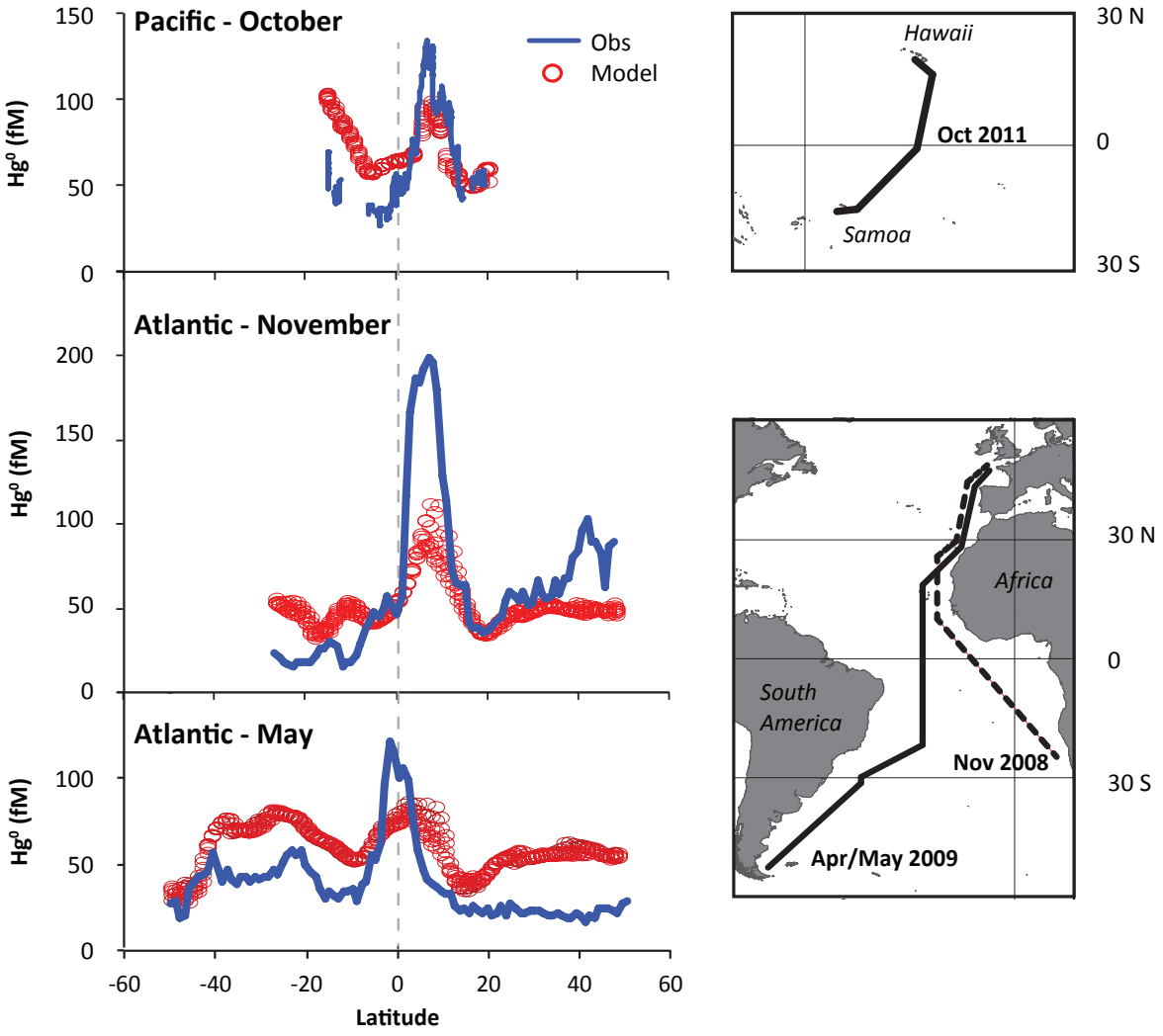

Figure 3. Comparison of modeled (red) and observed (blue) latitudinal gradients in Hg^0 along cruise tracks in the Pacific and the Atlantic Oceans. Model results are from the MITgcm within ±2 degrees of the cruise track with atmospheric inputs from the GEOS-Chem global Hg model. Data from the Atlantic Ocean are from *Kuss et al.*[16]

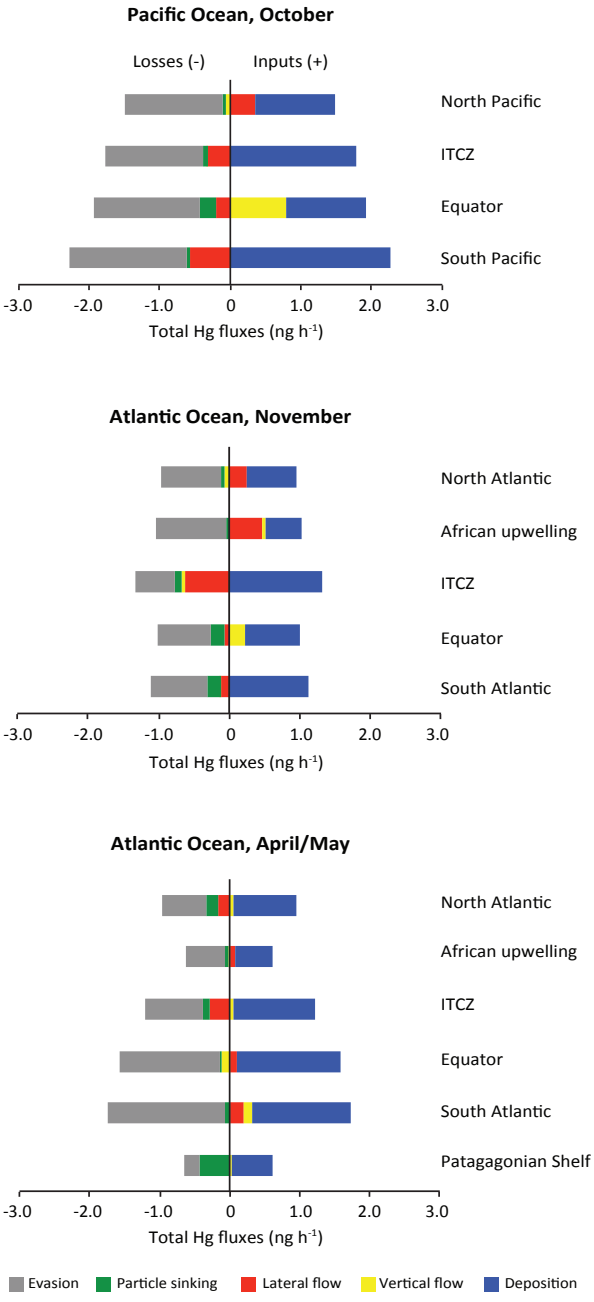

Figure 4. Modeled inputs and losses of Hg in the ocean mixed layer across the cruise regions sampled. Results are presented as monthly averages from the MITgcm Hg simulation.29 Model comparison with observations indicates a low bias in atmospheric inputs in the ITCZ (Figure 3). Specifications of the budget calculations reported here are provided in the SI.

502